Observation of a multimode quasi-normal spectrum from a perturbed black hole

Collin D. Capano[1,2*]**, Miriam Cabero**[3]**, Jahed Abedi**[1,2]**, Shilpa Kastha**[1,2]**, Julian Westerweck**[1,2]**, Alexander H. Nitz**[1,2]**, Alex B. Nielsen**[4]**, Badri Krishnan**[1,2,5]

[1] Albert-Einstein-Institut, Max-Planck-Institut für Gravitationsphysik, Callinstraße 38, 30167 Hannover, Germany,

[2] Leibniz Universität Hannover, 30167 Hannover, Germany,

[3] Department of Physics and Astronomy, The University of British Columbia, Vancouver, BC V6T 1Z4, Canada,

[4] Department of Mathematics and Physics, University of Stavanger, NO-4036 Stavanger, Norway,

[5] Institute for Mathematics, Astrophysics and Particle Physics, Radboud University, Heyendaalseweg 135, 6525 AJ Nijmegen, The Netherlands.

ABSTRACT

We provide strong observational evidence for a multimode black hole ringdown spectrum, using the gravitational wave event GW190521. We show strong evidence for the presence of at least two ringdown modes, with a Bayes factor of $43.4^{+8.1}_{-6.8}$ preferring two modes over one. The dominant mode is the fundamental $\ell = m = 2$ harmonic, and the sub-dominant mode corresponds to the fundamental $\ell = m = 3$ harmonic. We estimate the redshifted mass and dimensionless spin of the final black hole as $332^{+31}_{-35}\,\mathrm{M}_\odot$ and $0.871^{+0.052}_{-0.096}$ respectively. The detection of the two modes disfavors a binary progenitor with equal masses, and the mass ratio is constrained to $0.45^{+0.22}_{-0.29}$. General relativity predicts that the frequency and damping time of each mode in the spectrum depends only on two parameters, the black hole mass and angular momentum. Consistency between the different modes thus provides a test of general relativity. As a test of the black hole no-hair theorem, we constrain the fractional deviation of the sub-dominant mode frequency from the Kerr prediction to $\delta f_{330} = -0.010^{+0.073}_{-0.121}$.

1 Introduction

A perturbed black hole approaches equilibrium by emitting a spectrum of damped sinusoidal gravitational wave signals[1–3]. Unlike other astrophysical objects, the ringdown spectrum of a black hole is remarkably simple. General relativity predicts that the frequencies and damping times of its entire ringdown spectrum are fully determined by just two numbers, the black hole mass, M, and angular momentum, J, as described by the Kerr solution[4]. This prediction, a consequence of the black hole "no-hair theorem", does not hold in many alternate theories of gravity. Thus, if astrophysical black holes are observed to violate this property, it indicates new physics beyond standard general relativity.[5]

In order to observationally test this prediction using binary black hole mergers, an important observational challenge must be met.[6] The higher the binary mass ratio asymmetry, the more likely it is that sub-dominant ringdown modes are observable. However, more asymmetric binary systems are less likely to be formed, and also lead to weaker signals. Population studies suggested that such multimode ringdown modes were unlikely to be observed until the next generation of gravitational wave observatories.[7, 9]

Here we confound this expectation with the gravitational wave event GW190521, detected by the two LIGO detectors and Virgo at 03:02:29 UTC on the 21st May, 2019.[10, 11] This is the heaviest black hole merger event observed to date.[12, 13] The signal is consistent with the merger of two high mass black holes which merge at a low frequency relative to the detector sensitivity band. As such it has a barely observable in-spiral and the signal is dominated by the merger and ringdown phase.

GW190521 was initially reported as the merger of two comparable mass black holes[10, 11], in which case one would not expect to detect sub-dominant ringdown modes. Subsequent re-analysis of the data suggested that the progenitor was in fact likely to be an intermediate mass-ratio binary,[14] suggesting the possibility of detectable sub-dominant modes. Here indeed, we find strong evidence for multimode damped sinusoids in the ringdown phase of the gravitational wave event GW190521.

2 Agnostic search

A quasi-normal mode description of the gravitational wave from a binary black hole is not expected to be valid until after the binary has merged to form a perturbed black hole. On the flip side, the damping time of an $O(100\,\mathrm{M}_\odot)$ black hole is $O(10\,\mathrm{ms})$, leaving a window of only a few tens of milliseconds after merger in which the ringdown is detectable above noise. Accurate identification of the merger time is therefore crucial to extract quasi-normal modes from the data. To account for uncertainty in the merger time of GW190521 due to modelling systematics, we perform a series of analyses in 6 ms increments starting at a geocentric GPS reference time $t_{\mathrm{ref}} = 1242442967.445$. The reference time is taken from the maximum likelihood geocentric time obtained via the NR Surrogate analysis in Nitz & Capano.[14] We also fix the sky location to the maximum likelihood values from the same analysis.
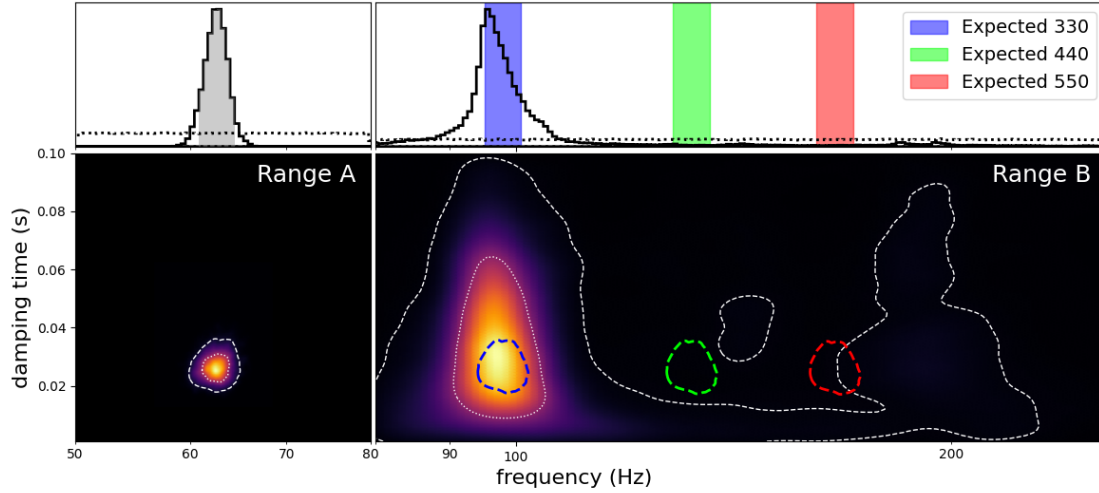
1

Figure 1. Marginal posterior probability distributions on frequency and damping time from an agnostic quasi-normal mode analysis of GW190521 at 6ms after $t_{\rm ref}$. A single mode is searched for in each of the shown frequency ranges, range A 50 to 80Hz and range B 80 to 256Hz. Top panels show the marginal posterior on the mode frequencies, with priors indicated by dotted lines; the gray region in the top left panel shows the highest 90th percentile density interval of the dominant mode. White dotted (dashed) contours in the bottom panels show the 50th (90th) credible regions. Assuming the dominant mode in range A corresponds to the (220) mode of a Kerr black hole, we estimate what the frequency and damping times would be of the (330), (440), and (550) modes (blue, red, and green regions, respectively). The mode in range B is clearly consistent with the expected frequency and damping time of the (330) mode.

The most agnostic way to search for quasi-normal modes from a perturbed black hole is to search for them individually, without assuming any relation between them. Such a search is complicated by the nature of quasi-normal modes: they are not orthogonal, meaning that modes that overlap in time must be sufficiently separated in frequency in order to be distinguishable. Simulations of binary black hole mergers have shown that one mode is typically significantly louder than the other modes. In order to extract sub-dominant modes from noisy data in an agnostic search it is necessary to separate the dominant mode in frequency from the others.

A visual inspection of the time- and frequency-domain data taken at the reference time revealed significant power in the two LIGO detectors between 60-70 Hz (see Supplemental Fig. S.1). In order to isolate this and search for sub-dominant modes we constructed three frequency ranges: "range A" between $50 - 80$ Hz, "range B" between $80 - 256$ Hz, and "range C" between $15 - 50$ Hz. We search for one quasi-normal mode in each range using Bayesian inference. We use uniform priors on the amplitudes of the modes in range B and C between 0 and 0.9 times the mode in range A. No other relation is assumed between the modes.

We repeat this analysis at time steps of $t_{\rm ref}+$ 0, 6, 12, 18, and 24 ms. As expected from the visual inspection of the data, we find a significant mode in range A at all grid points, which decreases in amplitude as we move to later times. A clear second mode is found in range B. This mode is most visible

at $t_{\rm ref} + 6$ ms, the result of which is shown in Fig. 1. The frequency of the secondary mode at this time is $97.7^{+97.5}_{-8.1}$ Hz with a damping time of 32^{+42}_{-26} ms, while the primary mode has frequency of $62.6^{+1.8}_{-2.0}$ Hz and damping time $26.4^{+7.9}_{-5.9}$ ms. The signal-to-noise ratio (SNR) of the primary and secondary modes of the maximum likelihood waveform is 12.2 and 4.1, respectively. Results from range C (not shown) are consistent with noise.

The ringdown spectrum of a Kerr black hole consists of an infinite set of frequencies $f_{\ell mn}$ and damping times $\tau_{\ell mn}$ labeled by three integers (ℓ, m, n). Here ℓ and m are the usual angular harmonic numbers. The third index $n \geq 0$ denotes overtones with $n = 0$ being the fundamental mode.

The dominant mode found at $62.6^{+1.8}_{-2.0}$ Hz is expected to be the quadrupolar $\ell = m = 2, n = 0$ fundamental mode. Measurement of f_{220} and τ_{220} provides an estimate of the mass and angular momentum of the remnant black hole. This in turn predicts the entire ringdown spectrum of subdominant modes. Figure 1 shows that the subdominant mode at $97.7^{+97.5}_{-8.1}$ Hz is consistent with $\ell = m = 3$ and $n = 0$. This is also in full agreement with expectations from numerical simulations of binary black hole mergers.[15, 16]

3 Consistency and deviations from Kerr

The search for damped sinusoids in section (2) assumed no particular relation between different modes, with a correspond-
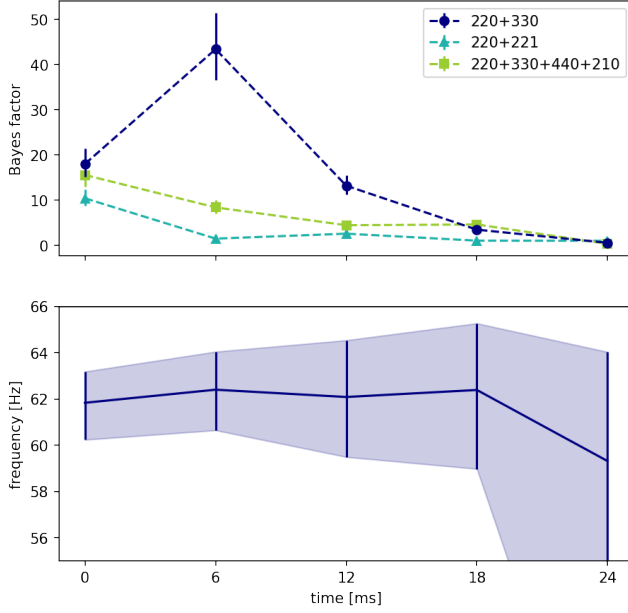
Figure 2. (*Top*) Bayes factor of models with the indicated modes compared to a model assuming the presence of only the (220) mode. All values are shown for five different start times of the analysis relative to the reference time $t_{\rm ref}$. (*Bottom*) Median values and 90% credible intervals for the (220) mode found when assuming a Kerr black hole ringdown model.

ing large prior parameter volume. In this section, we assume that the frequency and damping time of each damped sinusoid are related as in the ringdown of a Kerr black hole. This has the effect of reducing the prior parameter volume and focusing in on particular modes.

The amplitudes and phases of the modes are left as free parameters, since they depend on the specific initial state of the remnant black hole immediately after the merger.

For this analysis, we assume that the agnostically found dominant mode near 63Hz is the (220) mode of a Kerr black hole and we make various choices for the identity of the sub-dominant mode. We also consider the possibility of finding more than two modes. Additionally, we make different choices for the start time of the ringdown relative to the reference time $t_{\rm ref}$, as described in section (2).

Results for various multi-mode Kerr models are shown in Figure 2. The preferred model is the combination of the (220) and (330) modes at 6ms after $t_{\rm ref}$, with a Bayes factor of $43.4^{+8.1}_{-6.8}$ compared to a model with a single (220) mode.

Only moderate evidence is found for the presence of any other modes, although at 18ms after $t_{\rm ref}$ the most favoured model is one containing the (220), (330), (440) and (210) modes.

Figure 2 also shows the (220) mode frequency, f_{220}, measured with the preferred Kerr model –(220) + (330) modes– at different ringdown start times. The stability of f_{220} indi-
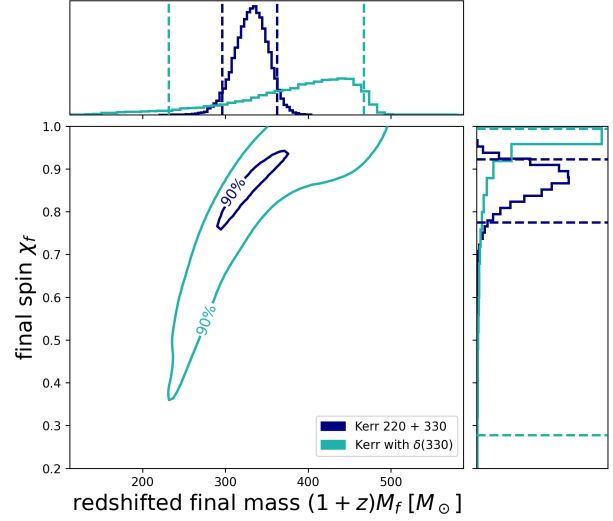

Figure 3. Posterior distribution of final redshifted mass $(1+z)M_f$ and dimensionless spin χ_f assuming the identified modes are the (220) and (330) modes of a Kerr black hole. Vertical dashed lines indicate the 90% credible interval. For the Kerr+δ(330) results, we use fitting formulae[8] to convert the frequency $f_{330}(1+\delta f_{330})$ and damping time $\tau_{330}(1+\delta\tau_{330})$ into mass and spin.

cates that the black hole has reached a regime of constant ringdown frequency. Figure 3 shows the final Kerr black hole mass, M_f, and dimensionless spin, $\chi_f = J_f/M_f^2$, measured with this model. We find that the remnant black hole has redshifted mass $(1+z)M_f = 332^{+31}_{-35}\,{\rm M}_\odot$ and dimensionless spin $\chi_f = 0.871^{+0.052}_{-0.096}$.

We now extend our analysis to consider deviations of the (330) parameters from the expected Kerr values. Thus, we extend the signal model keeping the dependence of f_{220} on (M,χ) as in the Kerr solution but including fractional deviations δf_{330} and $\delta\tau_{330}$ of f_{330} and τ_{330}, respectively. This is the classic no-hair theorem test.[6] Figure 3 shows the Kerr black hole mass M_f and dimensionless spin χ_f associated to this (330) mode frequency $f_{330}(1+\delta f_{330})$ and damping time $\tau_{330}(1+\delta\tau_{330})$. Posterior distributions on these parameters are shown in Supplemental Fig. S.4. We constrain the fractional deviation from Kerr to $\delta f_{330} = -0.010^{+0.073}_{-0.121}$. The damping time is only weakly constrained, $\delta\tau_{330} = 0.7^{+1.9}_{-1.3}$. We obtain slightly better constraints when we include the (440) and (210) modes in the analysis (see Supplemental Fig. S.5), however, this model is only marginally favored over the (220)+(330) at 18ms, and disfavored at all earlier times.

4 Discussion and comparison with previous results

The detection of a (330) mode indicates that the progenitor black holes in GW190521 had asymmetric masses, since
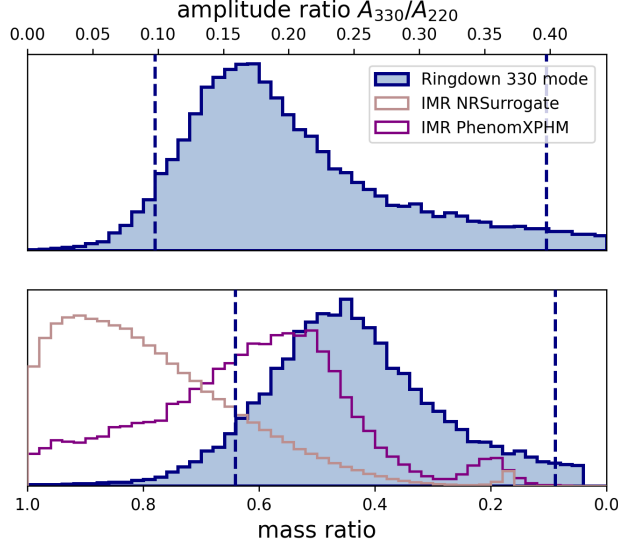
Figure 4. Posterior distribution for *(top)* the amplitude ratio of the (330) mode, A_{330}/A_{220}, and *(bottom)* the mass ratio of the binary, $m_2/m_1 < 1$, obtained using numerical fits between the (330) amplitude and mass ratio.[16] Vertical dashed lines indicate the 90% credible interval. For comparison, we also show the mass ratio obtained from the full signal using NR Surrogate[14] and PhenomXPHM models (see Supplemental Sec. 7.1), reweighted to a uniform prior in mass ratio between $[1/25, 1]$.

equal-mass binaries are not expected to excite the (330) mode. Figure 4 shows the posterior distribution on the amplitude of the (330) mode and on the ratio of the initial black hole masses m_1 and m_2 using numerical fits between the (330) amplitude and mass ratio.[16] We find $m_2/m_1 = 0.45^{+0.22}_{-0.29}$.

The redshifted final mass and spin of GW190521 were found by the LVC using a (220) ringdown fit to be $(1+z)M_f = 282.2^{+50.0}_{-61.9}M_\odot$, or $259.2^{+36.6}_{-29.0}M_\odot$ when analyzing the full signal.

The low-mass-ratio part of the posterior of Nitz and Capano[14] found $(1+z)M_f \sim 260M_\odot$ using the full signal.[17,18]

These results are somewhat in tension with the final mass and spin inferred from the ringdown modes found here. The complete waveform models used in the above analyses still do not include all relevant physical effects, for instance eccentricity. This, coupled with the fact that GW190521 has a very short inspiral signal, can lead to systematic errors for parameter estimation. On the other hand, the ringdown waveforms used in this paper are simpler and more robust for signals like GW190521, provided they are applied sufficiently late in the post-merger regime. This argument would tend to favor the estimates derived in this paper for the total mass. Nevertheless, a satisfactory resolution of this tension provides a valuable challenge for both approaches.

Overtones were found in the ringdown phase of GW150914[19] and GW190521_074359[20] (not to be confused

with GW190521). Black hole spectroscopy tests showed consistency with the Kerr hypothesis for these events.[19–21] These results rely on modeling the entire post-merger signal, starting immediately after the merger, by a combination of ringdown modes including the higher ringdown overtones with $n \geq 1$. There is however as yet no fundamental argument or calculation from general relativity that shows the remnant black hole is in the perturbative regime even immediately after its formation.

Moreover, following-up from early work due to Nollert and Price[22,23], recent work[24–26] has shown that the higher overtones are unstable even under extremely small, high-frequency perturbations of the effective potential. While the applicability of this work to astrophysical black holes is not yet fully clear, it shows that it would be preferable if black hole spectroscopy could be carried out without the higher overtones. Furthermore, since the overtones frequencies are very close to each other, it is difficult to resolve them individually and thus they cannot achieve a comparable precision to our results here.

The true nature of the gravitational wave event GW190521 has been the subject of much speculation.[27–29] The interpretation of GW190521 as a head-on collision of two highly spinning Proca stars[29] predicts the presence of a (200) mode[30], which is strongly disfavored by our results. Additionally, the high mass multiple mode ringdown signal observed here does not agree with the scenario of a very massive star collapsing to a black hole of mass $\sim 50M_\odot$ and an unstable massive disk.[31]

Expectations based on population models were that black hole ringdown signals with multiple modes were unlikely to be observed with the Advanced LIGO and Virgo detectors[7,9] (although those population models did not include massive binaries). Our results here show that, remarkably, GW190521 displays distinct subdominant modes and that these modes are consistent with the ringdown of a Kerr black hole.

5 Methods

5.1 The ringdown signal model

The quasi-normal mode (QNM) spectrum of allowed frequencies $\omega_{\ell mn}$ and damping times $\tau_{\ell mn}$ of a perturbed Kerr black hole are labeled by three integers $\ell = 2, 3, \ldots$, $-\ell \leq m \leq \ell$, and $n = 0, 1, 2, \ldots$. These can be combined together in a complex frequency $\Omega_{\ell mn} = \omega_{\ell mn} + i/\tau_{\ell mn}$ such that the ringdown signal of a perturbed Kerr black hole can be expressed as a sum of damped sinusoids:

$$h_+ + ih_\times = \frac{M_f}{D_L} \sum_{\ell mn} {}_{-2}S_{lm}(\iota, \varphi) A_{\ell mn} e^{i(\Omega_{\ell mn}t + \phi_{\ell mn})}, \quad (1)$$

where h_+ and $h_\times$ are the plus and cross polarizations of the gravitational wave, M_f is the mass of the black hole in the detector frame and D_L is the luminosity distance to the source. The functions ${}_{-2}S_{lm}(\iota, \varphi)$ are the spin-weighted spheroidal harmonics of spin weight -2, which depend on the inclination angle ι between the black hole spin and the line-of-sight from the observer to the source, and the azimuth angle φ between the black hole and the observer.

The complex QNM frequencies $\Omega_{\ell mn}$ can be determined from the Teukolsky equation[32,33]. By the no-hair theorem, the frequencies and damping times are determined by the mass M_f and spin χ_f of the black hole, with $\chi_f \in (-1,1)$. Positive (negative) spin means the perturbation is co-(counter-)rotating with respect to the black hole. The amplitudes $A_{\ell mn}$ and phases $\phi_{\ell mn}$ depend on the initial perturbation and take different values for different ℓmn modes.

For a given ℓ and n, the $+m$ and $-m$ modes are related to each other by $\Omega_{\ell-mn} = -\Omega_{\ell mn}$ and $\tau_{\ell-mn} = \tau_{\ell mn}$[8]. Furthermore, if the ringdown waveform is circularly polarized, the amplitude and phase of the $\pm m$ modes are related to each other by $A_{\ell-mn}e^{i\phi_{\ell-mn}} = -(1)^\ell A_{\ell mn}e^{-i\phi_{\ell mn}}$. By "circularly polarized", we mean that an observer at an inclination angle of 0 or π (above or below the black hole, as determined by the direction of its spin) would detect gravitational waves in which the plus and cross polarizations have equal amplitudes; the polarization for observers at other positions are determined by the spheroidal harmonics.

Numerical simulations of black hole binaries have shown that it is difficult to get non-circular polarization in the ringdown[8]. To simultaneously sum over the $\pm m$ modes for a given ℓn, we parameterize the waveform as

$$
\begin{aligned}
h_{\ell|m|n} = A^0_{\ell|m|n}e^{-t/\tau_{\ell|m|n}} \times \\
\left[_{-2}S_{\ell mn}(\iota,\varphi)A^{(+)}_{\ell|m|n}e^{i(\Omega_{\ell|m|n}t+\phi_{\ell|m|n})} \right. \\
\left. + _{-2}S_{\ell-mn}(\iota,\varphi)A^{(-)}_{\ell|m|n}e^{-i(\Omega_{\ell|m|n}t-\phi_{\ell|m|n})} \right],
\end{aligned}
$$

where, $A^0_{\ell|m|n}$ is the intrinsic amplitude of the (ℓmn) mode and

$$A^{(+)}_{l|m|n} = \sqrt{2}\cos(\pi/4 + \Delta\beta_{l|m|n}) \tag{2}$$

$$A^{(-)}_{l|m|n} = \sqrt{2}\sin(\pi/4 + \Delta\beta_{l|m|n})e^{i(l\pi+\Delta\phi_{l|m|n})}. \tag{3}$$

If the parameters $\Delta\beta_{\ell mn}$ and $\Delta\phi_{\ell mn}$ are both zero, the waveform reduces to circular polarization.

For all Kerr analyses, we do two analyses, a circularly polarized one in which $\Delta\beta_{\ell mn}$ and $\Delta\phi_{\ell mn}$ are both set to zero, and one in which a common $\Delta\beta$ and $\Delta\phi$ for all modes are allowed to vary uniformly between $[-\pi/4,\pi/4]$ and $[-\pi,\pi]$, respectively. In all cases we find that the circularly polarized analysis is favored over the arbitrary polarized analysis; we therefore only report results from the former here. In all analyses we fix $\varphi = 0$, as it is degenerate with modes' initial phases. To obtain the frequency and damping times for a given mass and spin we use tabulated values from Berti et al.[8], which we interpolate using a cubic spline. For the spheroidal harmonics we use tabulated values of the angular separation constants (also from Berti et al.[8]) and solve the recursion formula given in Leaver[33]. Our code for doing this is publicly available on GitHub[38].

For the agnostic analysis, we do not assume any mode corresponds to any particular ℓmn. We therefore use arbitrary complex numbers $X_{\ell\pm mn} = e^{i\psi_{\ell\pm mn}}$ in place of the $_{-2}S_{\ell\pm mn}$. Here, the $\psi_{\ell\pm mn}$ are allowed to vary uniformly in $[0,2\pi)$. We

vary a common $\Delta\beta$ parameter, but fix the $\Delta\phi$ parameter to zero, as it is degenerate with the $X_{\ell mn}$.

5.2 Analysis methods

We use the open source PyCBC Inference library for computational analysis.[39,40] To avoid contamination from the loud merger signal we remove the inspiral-merger contributions by "gating" them out. This is accomplished by zeroing the residual $d(t) - h(t)$ over a two second window (or "gate") ending at the analysis start time, where $d(t)$ and $h(t)$ are the data and template waveform, respectively. The gated region of time is then "in painted" such that the contribution to the likelihood from the gated region is zero.[41] We use data for the event GW190521 made publicly available by the Gravitational Wave Open Science Center.[36] We choose to fix the sky location to the values given by the maximum likelihood result of Nitz and Capano,[14] although we have obtained similar results using the LVC's maximum likelihood sky location.[11] We use a geocentric GPS reference time of $t_{\text{ref}} = 1242442967.445$.[14] Credible intervals in the text are quoted to 90%.

6 Acknowledgments

References

1. C. V. Vishveshwara, "Scattering of Gravitational Radiation by a Schwarzschild Black-hole", Nature **227**, 936–938 (1970)

2. S. Chandrasekhar and S.L. Detweiler, "The quasi-normal modes of the Schwarzschild black hole", Proc. Roy. Soc. Lond. A **344** (1975), 441–452"

3. B. P. Abbott *et al.*, "Tests of general relativity with GW150914," Phys. Rev. Lett. **116**, 221101 (2016) [erratum: Phys. Rev. Lett. **121**, no.12, 129902 (2018)]

4. R. P. Kerr, "Gravitational field of a spinning mass as an example of algebraically special metrics," Phys. Rev. Lett. **11** (1963), 237-238

5. V. Cardoso and P. Pani, "Testing the nature of dark compact objects: a status report," Living Rev. Rel. **22** (2019) no.1, 4

6. O. Dreyer *et al.*, "Black hole spectroscopy: Testing general relativity through gravitational wave observations," Class. Quant. Grav. **21** (2004), 787-804

7. E. Berti, A. Sesana, E. Barausse, V. Cardoso and K. Belczynski, "Spectroscopy of Kerr black holes with Earth- and space-based interferometers," Phys. Rev. Lett. **117** (2016) no.10, 101102

8. E. Berti, V. Cardoso and C. M. Will, "On gravitational-wave spectroscopy of massive black holes with the space interferometer LISA," Phys. Rev. D, **73** (2006), 064030

9. M. Cabero *et al.*, "Black hole spectroscopy in the next decade," Phys. Rev. D **101** (2020) no.6, 064044

10. R. Abbott *et al.* [LIGO Scientific and Virgo], "GW190521: A Binary Black Hole Merger with a Total Mass of 150$M_\odot$," Phys. Rev. Lett. **125** (2020) no.10, 101102

11. R. Abbott *et al.* [LIGO Scientific and Virgo], "Properties and Astrophysical Implications of the 150 $M_\odot$ Binary Black Hole Merger GW190521," Astrophys. J. Lett. **900** (2020) no.1, L13

12. R. Abbott *et al.* [LIGO Scientific and Virgo], "GWTC-2: Compact Binary Coalescences Observed by LIGO and Virgo During the First Half of the Third Observing Run," [arXiv:2010.14527 [gr-qc]].

13. A. H. Nitz *et al,* "2-OGC: Open Gravitational-wave Catalog of binary mergers from analysis of public Advanced LIGO and Virgo data," Astrophys. J. **891**, 123

14. A. H. Nitz and C. D. Capano, "GW190521 may be an intermediate mass ratio inspiral," Astrophys. J. Lett. **907** (2021) no.1, L9

15. I. Kamaretsos, M. Hannam, S. Husa and B. S. Sathyaprakash, "Black-hole hair loss: learning about binary progenitors from ringdown signals," Phys. Rev. D **85** (2012), 024018

16. S. Borhanian, K. G. Arun, H. P. Pfeiffer and B. S. Sathyaprakash, "Comparison of post-Newtonian mode amplitudes with numerical relativity simulations of binary black holes," Class. Quant. Grav. **37** (2020) no.6, 065006

17. V. Varma *et al.*, "Surrogate model of hybridized numerical relativity binary black hole waveforms," Phys. Rev. D **99** (2019) no.6, 064045

18. G. Pratten *et al.*, "Let's twist again: computationally efficient models for the dominant and sub-dominant harmonic modes of precessing binary black holes," [arXiv:2004.06503 [gr-qc]].

19. M. Isi, M. Giesler, W. M. Farr, M. A. Scheel and S. A. Teukolsky, "Testing the no-hair theorem with GW150914," Phys. Rev. Lett. **123** (2019) no.11, 111102

20. R. Abbott *et al.* [LIGO Scientific and Virgo], "Tests of General Relativity with Binary Black Holes from the second LIGO-Virgo Gravitational-Wave Transient Catalog," [arXiv:2010.14529 [gr-qc]].

21. C. D. Capano and A. H. Nitz, "Binary black hole spectroscopy: a no-hair test of GW190814 and GW190412," Phys. Rev. D **102** (2020) no.12, 124070

22. H.P. Nollert, "About the significance of quasinormal modes of black holes", Phys. Rev. D, **53** (1996), 4397–4402".

23. H.P. Nollert and R. Price, "Quantifying excitations of quasinormal mode systems", J. Math. Phys. **40** (1999), 980–1010.

24. J.L. Jaramillo, P. Macedo and L. Al Sheikh, "Pseudospectrum and black hole quasi-normal mode (in)stability", To appear in Phys. Rev. X [arXiv:2004.06434 [gr-qc]].

25. R.G. Daghigh, M.D. Green and J.C. Morey, "Significance of Black Hole Quasinormal Modes: A Closer Look", Phys. Rev. D **101** (2020), 104009

26. W. Qian, K. Lin, C. Shao, B. Wang and R. Yue, "Asymptotical quasinormal mode spectrum for piecewise approximate effective potential", Phys. Rev. D **103** (2021), 024019

27. J. Sakstein, D. Croon, S. D. McDermott, M. C. Straight and E. J. Baxter, "Beyond the Standard Model Explanations of GW190521," Phys. Rev. Lett. **125** (2020) no.26, 261105

28. M. Safarzadeh and Z. Haiman, "Formation of GW190521 via gas accretion onto Population III stellar black hole remnants born in high-redshift minihalos," Astrophys. J. Lett. **903** (2020) no.1, L21

29. J. C. Bustillo *et al.*, "GW190521 as a Merger of Proca Stars: A Potential New Vector Boson of 8.7×10^{-13} eV," Phys. Rev. Lett. **126** (2021) no.8, 081101

30. C. Palenzuela, I. Olabarrieta, L. Lehner and S. L. Liebling, "Head-on collisions of boson stars," Phys. Rev. D **75** (2007), 064005

31. M. Shibata *et al.*, "Alternative possibility of GW190521: Gravitational waves from high-mass black hole-disk systems," Phys. Rev. D **103** (2021) no.6, 063037

32. S. A. Teukolsky, "Rotating black holes - separable wave equations for gravitational and electromagnetic perturbations," Phys. Rev. Lett. **29** (1972), 1114-1118

33. E. W. Leaver, "An Analytic representation for the quasi normal modes of Kerr black holes," Proc. Roy. Soc. Lond. A **402** (1985), 285-298

34. R. Abbott *et al.* [LIGO Scientific and Virgo], "GW190412: Observation of a Binary-Black-Hole Coalescence with Asymmetric Masses," Phys. Rev. D **102** (2020) no.4, 043015

35. R. Abbott *et al.* [LIGO Scientific and Virgo], "GW190814: Gravitational Waves from the Coalescence of a 23 Solar Mass Black Hole with a 2.6 Solar Mass Compact Object," Astrophys. J. Lett. **896** (2020) no.2, L44

36. R. Abbott *et al.* [LIGO Scientific and Virgo], "Open data from the first and second observing runs of Advanced LIGO and Advanced Virgo," [arXiv:1912.11716 [gr-qc]].

37. I. M. Romero-Shaw, P. D. Lasky, E. Thrane and J. C. Bustillo, "GW190521: orbital eccentricity and signatures of dynamical formation in a binary black hole merger signal," Astrophys. J. Lett. **903** (2020) no.1, L5

38. Capano, C. D., 2021, pykerr, https://github.com/cdcapano/pykerr, GitHub

39. Nitz, A. H., *et al.* 2018b, PyCBC Software, https://github.com/gwastro/pycbc, GitHub

40. C. M. Biwer *et al.*, "PyCBC Inference: A Python-based parameter estimation toolkit for compact binary coalescence signals," Publ. Astron. Soc. Pac. **131** (2019) no.996, 024503

41. B. Zackay, T. Venumadhav, J. Roulet, L. Dai and M. Zaldarriaga, "Detecting Gravitational Waves in Data with Non-Gaussian Noise," [arXiv:1908.05644 [astro-ph.IM]].

7 Supplemental

7.1 Note on PhenomXPHM posterior samples

Posterior samples for GW190521 using the PhenomXPHM model[18] are obtained using a recently available updated implementation which allows for transitional precession. The analysis is performed in the same manner as in Nitz & Capano[14]. The updated model has reduced support for the most extreme mass ratio mode.
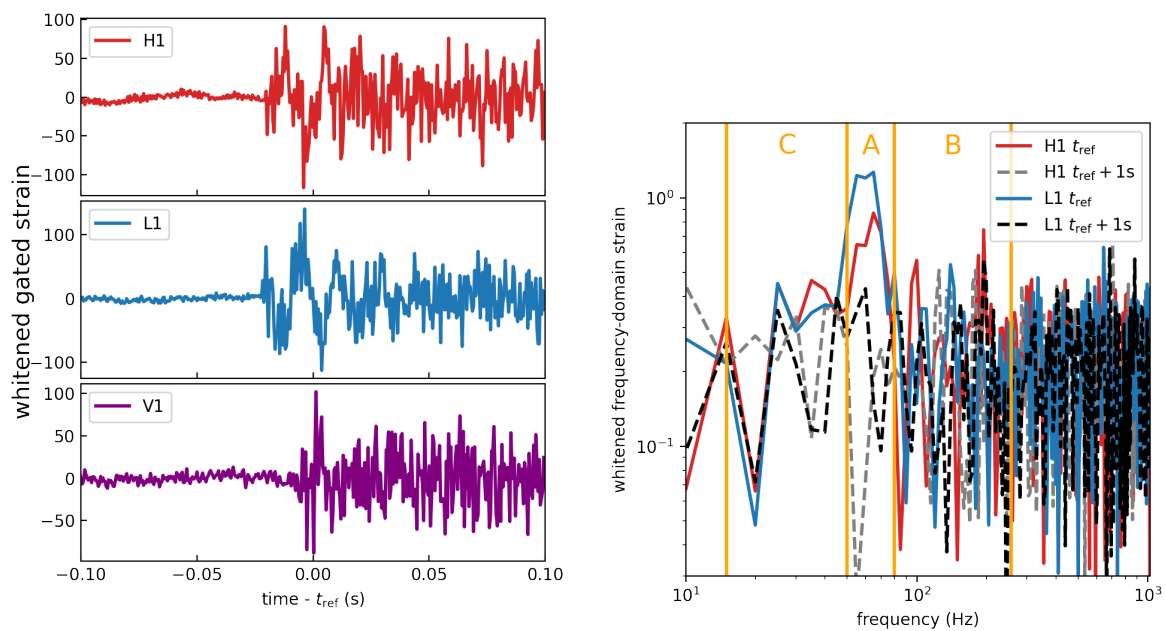
Figure S.1. *Left:* Whitened data in each detector, which have been gated at the reference time t_{ref}. *Right:* Frequency domain representation of the Hanford and Livingston data shown in the left panel. Also shown is the frequency domain representation of at an off-source time, one second later. The signal is clearly visible in the LIGO time-domain data, and is seen as a spike in the frequency domain data between $\sim 60 - 70\,\text{Hz}$. The primary frequency range's ("A") boundaries were set to isolate this spike. Frequencies below (region "C") and above (region "B") were searched for additional QNM in the agnostic analysis.
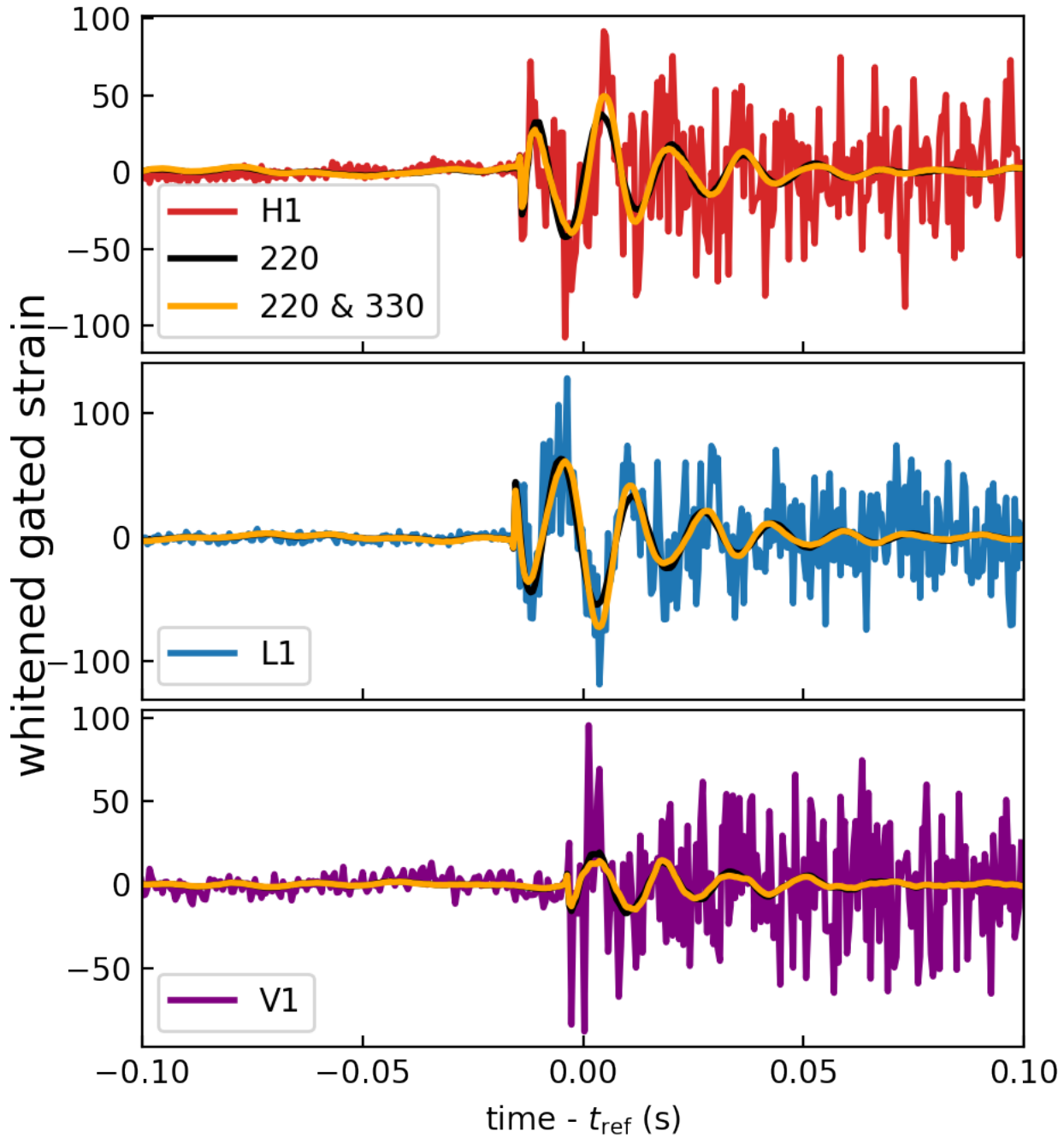
Figure S.2. Whitened data in each detector, with a gate applied at $6\,\mathrm{ms}$ after the reference time t_{ref}. Plotted are the maximum likelihood waveforms using just the (220) mode (black) and the (220) and (330) mode (orange). The model including the (330) mode is favored over the (220) mode by a Bayes Factor of $43.4^{+8.1}_{-6.8}$.
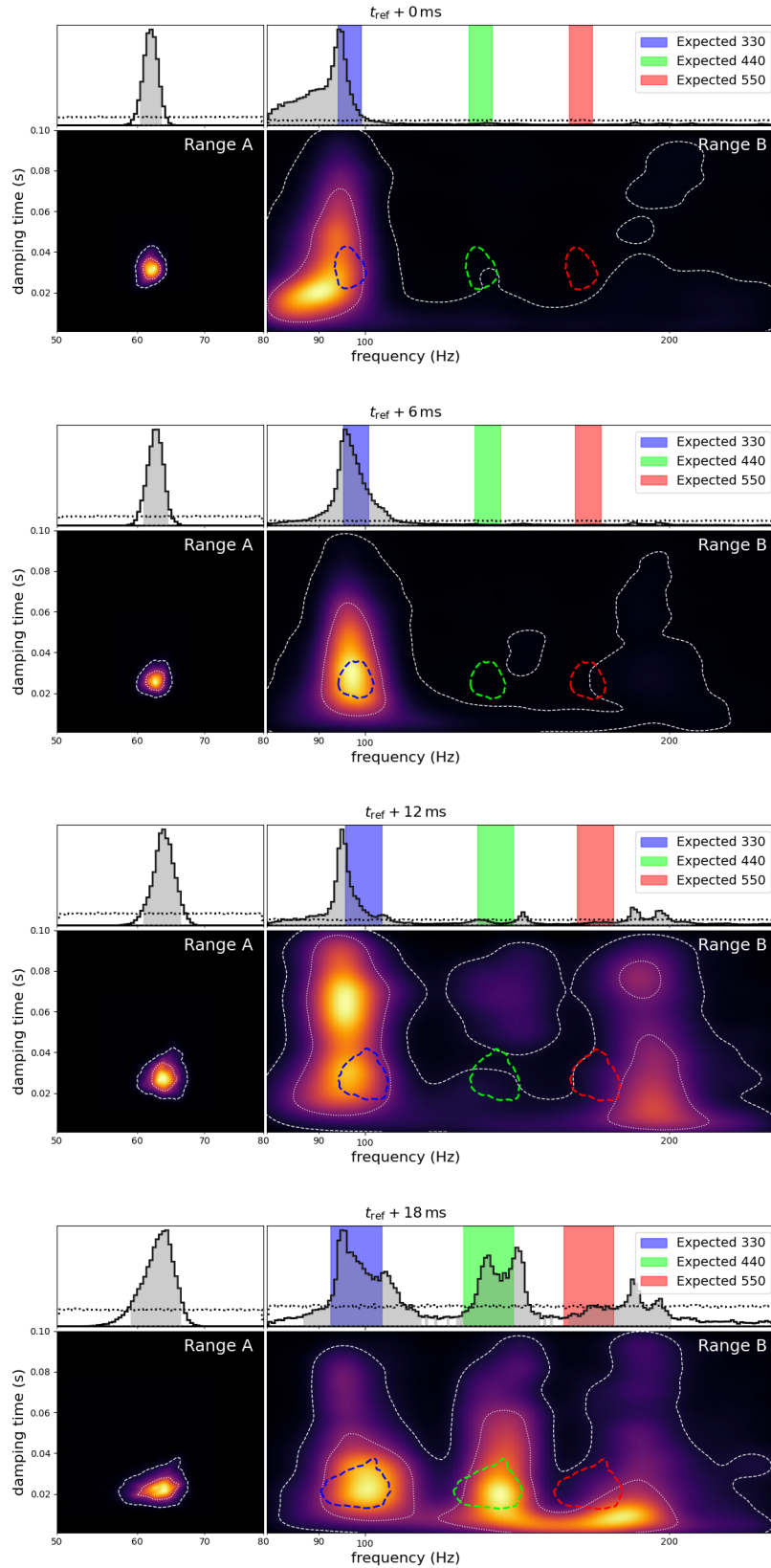
Figure S.3. Spectra plots at 0, 6, 12, and 18ms showing marginal posterior distributions from frequency range A and B in the agnostic analysis. Also shown are the expected regions for the 3,3 (blue), 4,4 (green), 5,5 (red) modes, assuming the peak in region A is the 2,2 mode.
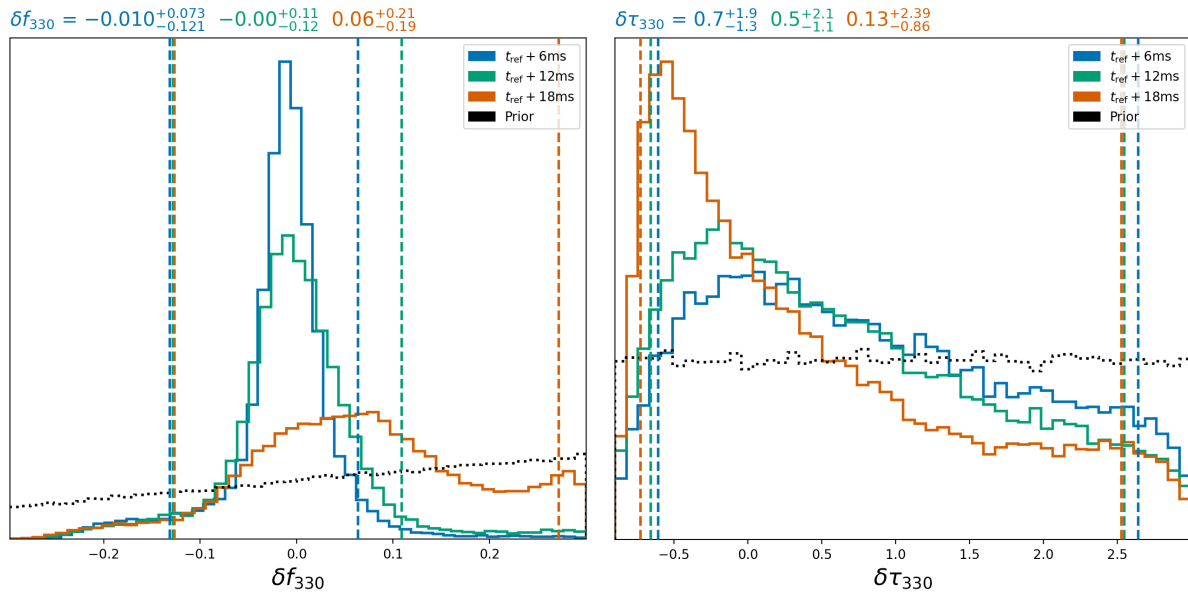
Figure S.4. Posterior on the deviation from Kerr of the (330) frequency δf_{330} (left) and damping time $\delta \tau_{330}$ (right) using a model in which we include the (220)+(330) modes at $t_{\text{ref}}+$ 6, 12, and 18ms. Quoted values are the median and 90% credible interval, which is indicated by the dashed vertical lines. We quote the values from the 6ms analysis in the main text, as the Bayes Factor for the presence of the (330) mode is highest at that point. We use a prior (black dotted lines) that is uniform over $\delta f_{330} \in [-0.3, 0.3)$, with the constraint that $f_{330}(1 + \delta f_{330}) > 75\,\text{Hz}$. This constraint is necessary to avoid label switching with the 220 mode; even with the constraint we clearly measure a lower bound on δf_{330}. For the damping time we use a prior that is uniform over $\delta \tau_{330} \in [-0.9, 3)$, and find that the damping time is only weakly constrained.
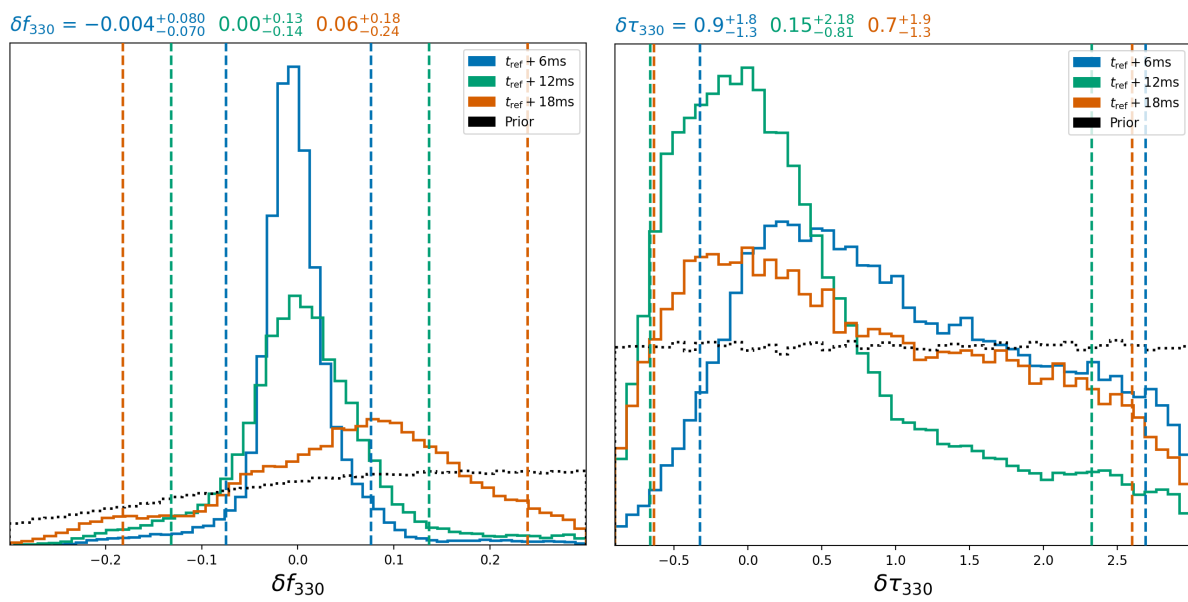
Figure S.5. Same as Fig. S.4, but using an analysis in which we include the (330), (440), and (210) modes, and allow them to deviate from their Kerr value. Shown are the resulting constraints on δf_{330} and $\delta \tau_{330}$. We find slightly tighter constraints at all times than in the analysis in which we only include the (220) and (330) modes. However, adding the (440) and (210) modes is only favored over a (220)+(330) analysis at $t_{\text{ref}} + 18 ms$.